Published in final edited form as:
Sci Transl Med. 2011 August 31; 3(98): 98ra83. doi:10.1126/scitranslmed.3002588.

A Computational Model to Predict the Effects of Class I Anti-Arrhythmic Drugs on Ventricular Rhythms

Jonathan D. Moreno[1,2], **Z. Iris Zhu**[2], **Pei-Chi Yang**[3], **John R. Bankston**[4], **Mao-Tsuen Jeng**[3], **Chaoyi Kang**[3], **Lianguo Wang**[3], **Jason D. Bayer**[5], **David J. Christini**[2], **Natalia A. Trayanova**[5], **Crystal M. Ripplinger**[3], **Robert S. Kass**[4], and **Colleen E. Clancy**[3,*]

[1]Tri-Institutional MD-PhD Program, Weill Cornell Medical College/The Rockefeller University/ Sloan-Kettering Cancer Institute, New York, NY 10021, USA

[2]Department of Physiology and Biophysics, Weill Medical College of Cornell University, 1300 York Avenue, New York, NY 10021, USA

[3]Department of Pharmacology, University of California, Davis, CA 95616–8636, USA

[4]Department of Pharmacology, Columbia University College of Physicians and Surgeons, 630 West 168th Street, New York, NY 10032, USA

[5]Department of Biomedical Engineering and Institute for Computational Medicine, The Johns Hopkins University, 3400 North Charles Street, CSEB, Room 216, Baltimore, MD 21218, USA

Abstract

A long-sought, and thus far elusive, goal has been to develop drugs to manage diseases of excitability. One such disease that affects millions each year is cardiac arrhythmia, which occurs when electrical impulses in the heart become disordered, sometimes causing sudden death. Pharmacological management of cardiac arrhythmia has failed because it is not possible to predict how drugs that target cardiac ion channels, and have intrinsically complex dynamic interactions with ion channels, will alter the emergent electrical behavior generated in the heart. Here, we applied a computational model, which was informed and validated by experimental data, that defined key measurable parameters necessary to simulate the interaction kinetics of the anti-arrhythmic drugs flecainide and lidocaine with cardiac sodium channels. We then used the model to predict the effects of these drugs on normal human ventricular cellular and tissue electrical activity in the setting of a common arrhythmia trigger, spontaneous ventricular ectopy. The model forecasts the clinically relevant concentrations at which flecainide and lidocaine exacerbate, rather than ameliorate, arrhythmia. Experiments in rabbit hearts and simulations in human ventricles based on magnetic resonance images validated the model predictions. This computational framework initiates the first steps toward development of a virtual drug-screening system that models drug-channel interactions and predicts the effects of drugs on emergent electrical activity in the heart.

[*]To whom correspondence should be addressed. ceclancy@ucdavis.edu.

Author contributions: J.D.M. designed and performed simulations, optimizations, and experiments, and prepared the manuscript; Z.I.Z. designed simulations; P.-C.Y. and M.-T.J. performed optimizations and analysis; J.R.B. and R.S.K. designed and performed experiments; C.K., L.W., and C.M.R. designed, performed, and analyzed optical mapping experiments; J.D.B. and N.A.T. designed and performed 3D modeling; D.J.C. assisted in manuscript preparation; C.E.C. designed simulations and experiments and prepared the manuscript.

Competing interests: The authors declare that they have no competing interests.

Introduction

One pharmacological approach for the management of lethal cardiac rhythms has been reduction of cellular excitability with sodium (Na) channel–blocking drugs. Reduction of Na current was anticipated to abolish irregular spontaneous electrical activity arising from disease-altered tissue after a heart attack. Although these drugs appeared to function exactly in this way in single-cell experiments (1, 2), the Cardiac Arrhythmia Suppression Trial (CAST) paradoxically showed that they caused a two- to threefold increase in sudden cardiac death compared to treatment with placebo (3, 4).

The failure of single-cell effects of anti-arrhythmic drugs to predict drug action in intact cardiac tissue does not, however, necessarily preclude their use (5). To determine the arrhythmic potential of existing or potential drugs, we have taken advantage of sophisticated models of ion channels (6) and the heart (7), together with high-performance computing, to develop a computational approach for predicting effects of anti-arrhythmic therapy (8). Our model incorporates current understanding of ion channel gating, time- and voltage-dependent drug-channel interaction (9), pH dependence of local anesthetics (10), modulated and guarded receptors (10–12), allosteric effects (13), and the clinical effects of Na channel–blocking drugs (14). This study builds on 50 years of research on mechanisms of drug-channel interactions (8). We therefore present a first step toward a computational framework that can be used to determine the conditions under which a specific drug will successfully prevent or exacerbate arrhythmia.

Results

The model

We began constructing our model by modifying and fitting a Markovian representation (6) of the cardiac Na channel that includes one conducting open state, three closed states, inactivated closed states, and fast- and slow-inactivated states to experimental data (figs. S1 and S2). To model drug binding, we assumed that any discrete state in the drug-channel model may be drug-free or drug-bound (10) (fig. S1). We used experimental data to determine access, diffusion (drug on rates), and channel conformation–specific affinity (drug off rates) for charged and neutral fractions of common anti-arrhythmic drugs, flecainide and lidocaine. Rate constants (fig. S3) were extracted from experimental data and used as initial guesses for numerical optimization, constrained by microscopic reversibility, and subjected to sensitivity analysis (fig. S5) (15) (Supplementary Material).

Channel kinetics determine situation-dependent blockade

Traditional classification of anti-arrhythmic drugs is based on drug association and dissociation kinetics (16) and reveals little about the effects of drugs on cardiac rhythms. Lidocaine, a class 1B anti-arrhythmic drug, has fast association and dissociation kinetics compared to flecainide, a prototypical class 1C drug with slow association and dissociation. Both the drug kinetics and specific contributions from charged and uncharged species are crucial in determining situation-dependent block of Na channels. Figure 1 summarizes drug-channel effects for flecainide (left) and lidocaine (right) as measured experimentally (symbols) and simulated by the model (lines).

Charged flecainide [98% at pH 7.4, pK_a = 9.3 (17)] rapidly diffuses into open Na channels (5830 M^{-1} ms^{-1}) (18) with high affinity [K_d at 0 mV (K_{d0}) = 11.2 μM] (19, 20). The neutral fraction (2%) has lower affinity (~400 μM) (17). Closed channels bind protonated and neutral flecainide with low affinity: K_d = ~100 μM (20, 21) and K_d = 794 μM (17), respectively. The affinity of the charged drug is intrinsically voltage-dependent ($K_d = K_{d0}e^{-dVF/(RT)}$) (22) for open and closed states, but the charged drug does not readily access

inactivated conformations (17). The neutral fraction, albeit small, binds with high inactivated state affinity (5.3 μM) (17), which caused a small but significant shift in experimentally measured steady-state availability (SSA) (−2.3 mV in the SSA curve; Fig. 1A, left).

Lidocaine is 60% charged at pH 7.4 [pK_a = 7.6 (17)] and diffuses at 330 M^{-1} ms^{-1} (23). Both charged and neutral fractions have low affinity to open channels [K_d at 0 mV (K_{d0}) = 318 μM (20) and K_d = 400 μM (23)]. Lidocaine has low affinity to closed [K_d = 895 μM (17)] channels. The neutral fraction binds with high affinity to inactivated states (3.4 μM) (17), resulting in a large left shift (−10.3 mV) of channel availability, which we reproduced in the computational model (Fig. 1A, right). Charged lidocaine does not bind inactivated channels.

In response to repetitive depolarization, Na channels exhibit use-dependent block (UDB) (17, 24), resulting from incomplete unblock during the interstimulus interval, determined by the off rate of the drug-complexed channel (11). Flecainide is predominantly charged at physiological pH and exhibited potent use dependence [experimental IC_{50} (median inhibitory concentration) = 11.2 μM at 5 Hz] (Fig. 1B, left) compared to lidocaine (experimental IC_{50} = 318 μM at 5 Hz) (Fig. 1B, right) in the experiment and simulation.

Flecainide and lidocaine profoundly slowed voltage-dependent channel recovery from UDB evoked by a long rapid pulse train (Fig. 1C). The complex recovery from 10 μM flecainide block during repolarization to −100 mV reflected several time-dependent processes (Fig. 1C, left). The initial phase (<10 ms) reflected closed-state recovery from block, the second (>10 ms and <1 s) was recovery from fast-inactivated state block (note the upward concavity arising from additional inactivation occurring during pulse 2), and the ultraslow phase (>1 s) was from recovery from a drug-trapped, inactivated state (25).

Recovery from UDB by 300 μM lidocaine at −100 mV occurred rapidly for more channels (~75%) in the two initial phases—from closed states and fast-inactivated states (Fig. 1C, right). Recovery from slow-inactivated state block by lidocaine was slow (>1 s) but constituted only ~25% of channels.

The frequency dependence of UDB for flecainide and lidocaine is shown in Fig. 1D, left and right, respectively. At rates 1 and 2 Hz, corresponding to 60 to 120 beats per minute (BPM), the degree of UDB by 10 μM flecainide (~30 to 40%) was greater than for 300 μM lidocaine (~10 to 20%). Profound buildup of flecainide-bound channels during repetitive pacing results from very slow drug unblock from drug-trapped inactivation states.

The dose dependence of tonic block in experiments and model is shown in Fig. 1E. A comparison of flecainide (left) and lidocaine (right) indicates higher affinity of flecainide for closed channels compared to lidocaine, indicated by tonic block.

Although such channel-level simulations informed determinants of pharmacokinetics, forecasting drug effects on the cellular action potential for specific drugs at varied drug concentrations and pacing frequencies was more challenging. Thus, we used our models of flecainide and lidocaine, which accurately recapitulate drug-channel interactions, to make predictions of drug effects in cells and tissues.

Effects of drugs on cellular excitability and conduction velocity

The concentration dependence of flecainide and lidocaine on single-cell (uncoupled) excitability (indicated by action potential maximum upstroke velocity) in the ten Tusscher human cardiac cell model (26) is shown in Fig. 2A. Cells were stimulated at 80 BPM with

concentrations of flecainide (left panel, 0.5 and 2 μM) (16) and lidocaine (right panel, 5 and 20 μM) corresponding to low and high clinical doses (16). High-dose lidocaine (20 μM) maintained upstroke velocity above 315 V/s, consistent with experiments (27), suggesting that therapeutic lidocaine minimally affects cardiac excitation. Therapeutic flecainide had disparate effects on excitability; 0.5 μM resembled lidocaine, whereas 2 μM substantially reduced upstroke velocity (<285 V/s). Flecainide (2 μM) reduced cellular excitability at normal frequency (60 and 80 BPM) and more at rapid rates (120 and 160 BPM indicative of human tachycardia) (Fig. 2B, left), comparable to observations in canine (28) and guinea pig (29) preparations. Conversely, even at high concentrations and pacing (20 μM, 160 BPM) of lidocaine, upstroke velocity was only decreased 35% in comparison to 60 BPM (Fig. 2B, right). Although single-cell cellular excitability was depressed by flecainide, successful action potentials were maintained, suggesting that flecainide is therapeutic because of its potential to suppress ectopic arrhythmia triggers by reducing excitatory Na current.

We next expanded our investigation to one-dimensional (1D) tissue representations of electrotonically coupled tissue and computed the effects of 0.5 and 2 μM flecainide at 120 BPM (red and green, respectively) and 2 μM flecainide at 160 BPM (tachycardia) (blue) on conduction velocity (CV) (Fig. 2C, left). Lidocaine (5 μM) at 120 BPM (red) and 20 μM lidocaine at 120 BPM (green) and 160 BPM (blue) are shown in Fig. 2C (right). For lidocaine and low-dose flecainide, CV was slowed, but successful, consistent with the single-cell simulations. However, for 2 μM (high dose in blue) flecainide, a marked reduction in CV occurred, and after 76 paced beats at 160 BPM, transient conduction block was observed. Consistent with previous studies (30), a substantial inhibition of I_{Na} (>95%) was required for conduction block. See fig. S7 for full excitation profiles and analysis of the onset of conduction block. Because of its high open-state affinity and very slow drug unblock (31), UDB by flecainide caused insufficient Na channel availability for successful conduction, a higher-dimensional phenomenon that emerged as a result of increased electrotonic load in coupled tissue.

Figure 2D shows threshold concentrations of flecainide (left) and lidocaine (right) for conduction block in a 100-cell 1D virtual tissue during static pacing. Conduction block did not occur at therapeutic lidocaine concentrations, whereas the high clinical dose for flecainide was dangerous during rapid pacing, because it set the stage for profound dispersion of refractoriness (repolarization). The maximum value of 180 BPM was comparable to a study of nonsustained ventricular tachycardia (average frequency, 193 ± 32 BPM) (32).

Experimental validation of model predictions

To validate our model predictions in cardiac tissue, we compared the computed effects of flecainide and lidocaine on conduction in our 1D virtual tissue to optical recordings in intact rabbit epicardium (Fig. 3). The model (100 coupled epicardial cells) (Fig. 3A) and the rabbit heart (Fig. 3B) were paced at 160 BPM for 5 min in the presence of 2 μM flecainide and 20 μM lidocaine. The model predicted the onset of conduction block at 160 BPM with 2 μM flecainide, which was confirmed at that concentration and frequency in the experiment. In both simulation and experiment, more conduction block occurred during the adaptation phase after drug application. Once conduction failed, a long recovery period [for example, diastolic interval (immediately after red arrows in Fig. 3)] allowed for drug unbinding and successful subsequent fast conduction (after red arrows, Fig. 3). Notably, application of a high clinical dose (20 μM) of lidocaine did not lead to conduction block in simulations (fig. S8) or experiments.

Vulnerability to arrhythmia

Na channel–blocking drugs were proposed to reduce cellular excitability and reduce spontaneous ventricular ectopy (3, 4, 33). The CAST study showed that although Na channel block reduced the number of spontaneous ventricular ectopic arrhythmogenic events (~80% event reduction), the pro-arrhythmic potential of the events that persisted was markedly exacerbated by drug blockade (3).

It has been long known that a period of vulnerability exists whereby electrical stimulation can initiate self-sustaining spiral waves (34, 35) capable of degeneration into fibrillatory rhythms. Thus, as in studies by Starmer et al. (11, 33, 36), we sought to systematically determine the likelihood of arrhythmia induced by spontaneous ventricular stimuli in clinically relevant concentrations of flecainide and lidocaine. 1D tissue simulations were used to assess the “vulnerable window” (VW) to unidirectional block and retrograde conduction, which suggests reentrant arrhythmia in higher dimensions (31, 36). The VW (Fig. 4A) indicates the time of arrhythmia susceptibility in response to spontaneous stimuli for a given drug concentration, pacing frequency (S1) (Fig. 4A, x axis), and spontaneous impulse timing (S2) (Fig. 4A, y axis) (protocol in Fig. 4B).

We ran simulations to determine the VW to unidirectional conduction block with 2 μM flecainide (Fig. 4C) (S1 = 120 BPM). A spontaneous impulse (S2) applied before the VW (blue dot in Fig. 4A, S1 – S2 = 438 ms) failed to excite refractory tissue (left). Two stimuli applied at the VW borders, the most premature beat (MPB) (red dot in Fig. 4A, S1 – S2 = 439 ms) and least premature beat (LPB) (green dot in Fig. 4A, S1 – S2 = 455 ms), led to successful retrograde propagation only, the hallmark of arrhythmogenic unidirectional conduction (S2 applied anywhere within the VW caused unidirectional conduction). An impulse applied after the VW (orange dot in Fig. 4A, S1 – S2 = 456 ms) led to bidirectional conduction. Notably, the velocity of the retrograde wave induced with flecainide was markedly slower than that with lidocaine (compare red and green dot frames in Fig. 4C to those in Fig. 4E). Both flecainide and lidocaine caused marked increases in the size of the VW compared to drug-free conditions (table S1). However, the size of the VW alone is not sufficient to predict arrhythmia risk.

To quantify drug-induced increase in arrhythmia risk, we used the Starmer metric (33) to compute the probability that an irregular stimulus can trigger reentry [*P*(Arrhythmia); see the Supplementary Material for details). Although the VW for 2 μM flecainide and 20 μM lidocaine was comparable at 120 BPM (16 and 15 ms, respectively), flecainide (black line, Fig. 4D) increased arrhythmia probability 12.2-fold compared to the drug-free condition, whereas lidocaine increased arrhythmia susceptibility by 6-fold (black line, Fig. 4F). This is because both the size of the VW and the cell refractory period determined arrhythmia likelihood. It is precisely the presumed anti-arrhythmic property of flecainide—decreased cell excitability (increased refractoriness)—that is profoundly pro-arrhythmic in coupled tissue. The steepness of black lines in Fig. 4D indicates escalating proclivity for arrhythmia with small increases in drug (use dependence) for flecainide but not for lidocaine (black line, Fig. 4F).

Emergent phenomena in 2D virtual tissue

Arrhythmia is fundamentally an emergent spatial phenomenon, so we used the 1D predictions to guide 2D simulations (Fig. 5) with high clinical drug concentrations (2 μM flecainide and 20 μM lidocaine) at 120 BPM. The predictions in 1D effectively scale to a 2D homogeneous virtual myocardium composed of 500 by 500 cells. To mimic an irregular beat, we applied a spontaneous impulse (S2) (after 500 paced beats initiated along the left edge of the tissue) (i) before, (ii) inside, or (iii) after the VW for flecainide (Fig. 5A) and

lidocaine (Fig. 5B). (See the Supplementary Material for pacing protocol.) Time snapshots (under panels) are shown for phase maps (37) after the last planar wave (S1) (first panel) through termination of the most persistent wave after S2 (last panel). Activation maps for each of the conditions are shown at the right.

For both flecainide and lidocaine, a spontaneous stimulus before the VW failed to propagate through refractory tissue (i). A spontaneous stimulus applied in the VW (ii) generated an arrhythmogenic reentrant wave with both drugs by propagating retrogradely and then turning and slowly reentering the tissue as it recovered from drug block. With lidocaine, reentry was short-lived because the fast-propagating wave caught its refractory tail (snapshot at 600 ms). Flecainide (2 μM) caused a persistent reentrant (>1.2 s) wave supported by slow conduction and consequent smaller reentrant core. The potential to sustain reentry stems from kinetics of recovery from drug block (31), which determines the degree of UDB and, consequently, CV. A spontaneous stimulus applied after the VW (iii) propagated in all directions and quickly died with both flecainide and lidocaine. The activation maps on the right illustrate the profound differences in rotor frequency between flecainide and lidocaine. During the VW, the flecainide-treated tissue required about 600 ms for the reentrant wave to make a full turn compared to 200 ms for lidocaine.

Experimental validation in whole hearts

The 2D model predictions were experimentally validated in rabbit epicardium. Figure 6 shows induction of arrhythmia observed experimentally with 2 μM flecainide. In response to cessation of burst pacing (Supplementary Material), a nonsustained transmural figure-of-eight reentry was initiated. Figure 6A shows optical maps of the rabbit epicardium, with white arrows indicating the path of excitation. The blue arrow (at 166 ms) indicates a transmural reentry of the wave tip, which reemerges in the epicardium (at 303 ms). The qualitative features of nonsustained reentry seen in the experiment (Fig. 6) were like those predicted by the computational model. Figure 6B shows the corresponding optical action potential recordings (site denoted by an asterisk in the first panel). Reentrant activity was never observed in experiments with clinically relevant doses of lidocaine.

Inherent differences in the experimental and simulated preparations (rabbit whole-heart optical mapping versus human 2D computational tissue model) prevented a direct quantitative comparison between the model predictions and the rabbit experiments. However, an analysis (details in the Supplementary Material) revealed analogous dynamics when the effective tissue sizes in the simulation and experiment were compared (38) in Figs. 5 and 6.

Simulations in 3D human ventricular models

Finally, to ensure that the model predictions in two dimensions hold true in more complex tissue structures, we tested flecainide and lidocaine in a magnetic resonance imaging (MRI)–based, anatomically detailed 3D model of the human ventricles (see Supplementary Material). After the VW was revealed as in Figs. 4 and 5, the 3D ventricles were paced from the apex at a rate of 120 BPM with high-dose flecainide (2 μM) (Fig. 7A) and high-dose lidocaine (20 μM) (Fig. 7B). An ectopic stimulus inside the VW (phase maps are shown) about halfway up the ventricles (~2.5 cm, consistent with Fig. 5) initiated a persistent figure-of-eight reentrant wave with flecainide (>2.5 s); in contrast, high-dose lidocaine induced one turn of reentry before dying out (<0.5 s). Consistent with the 2D results (Fig. 5), the lidocaine reentry was short-lived because the fast-propagating wave caught its refractory tail (videos S1 and S2).

Drug effects in heart failure

It is well known that spontaneous ventricular ectopy occurs more frequently for patients with heart failure (HF), as evidenced in the CAST study (3, 4, 14). We therefore explored the effects of drugs on HF myocardium on the basis of existing human data (model details in the Supplementary Material) (Fig. 8). We validated the HF model by comparing action potential duration (APD) and morphology (Fig. 8A) to the Priebe-Beuckelmann model (Fig. 8B) (39) and to measurements from human HF ventricular myocytes (40–42). Our HF model had an APD of 562.5 ms, comparable to recent experiments (477 to 506 ms) (41) and the Priebe-Beuckelmann model (548 ms) (39). We computed single-cell upstroke velocity (Fig. 8, C and D) and computed the minimum drug concentration that caused conduction block in 1D tissue (Fig. 8, E and F). The model predicted marked depression of single-cell excitability compared to normal tissue. This is a result of the additive effects of action potential prolongation, resulting in reduction in diastolic interval and, consequently, Na current, because of less recovery from inactivation and less recovery from drug block. At frequencies >140 BPM, the long HF action potential failed to adapt. Additional effects of HF-induced cellular uncoupling (see table S1) further exacerbate arrhythmia susceptibility by markedly reducing CV. This results in conduction block at slower frequencies and lower concentrations of both flecainide and lidocaine compared to normal tissue (Fig. 2).

In the HF setting, the VW does not constitute a reliable metric for prediction of arrhythmia induction by spontaneous ventricular ectopy, because of the potential for extremely slow Ca^{2+}-supported conduction (43, 44). We postulated that flecainide in HF would slow conduction so markedly that a spontaneous ventricular ectopic beat generated after the VW would lead to slow bidirectional conduction and generate a figure-of-eight reentry. Indeed, flecainide (1 μM) with a late ectopic beat induced a bidirectional figure-of-eight reentry that persisted for almost 4 s (Fig. 8G). This is in contrast to Fig. 5, in which the bidirectional wavefronts collide and die out. The HF reentry is due to extreme slowing of conduction and Ca^{2+}-mediated conduction of the initial wave propagation, which gives the Na channels time to recover and drive reentry. In contrast, lidocaine-blocked Na channels (Fig. 8H) recovered faster from drug blockade, preventing reentry. Notably, with lidocaine, bidirectional conduction lasted twice as long as in normal myocardium (Fig. 5).

Discussion

Drug-induced cardiac toxicity as a consequence of cardiac arrhythmia treatment burdens clinical arrhythmia management and stems in part from inadequate prediction of pro-arrhythmic potential. The CAST study showed that flecainide and encainide (both class 1C anti-arrhythmics) were two to three times more likely to cause arrhythmia than placebo and increased risk of sudden cardiac death in post-infarction patients (3, 4). Twenty years after the CAST study, the exact mechanism underlying flecainide's pro-arrhythmic potential is still unknown (27). There is also no way to quickly discriminate between drugs that slow conduction or widen the QRS complex (such as flecainide) and those that have a strong safety profile (such as lidocaine) (27). Our study describes a potential strategy to determine preliminary safety profiles of drugs that cause conduction slowing and widening of the QRS complex. Here, we tested prototypical anti-arrhythmic agents (flecainide and lidocaine), but the approach can be extended to predict pro-arrhythmic potential of other anti-arrhythmic agents—those currently in use, and those under development. Because efficient methods for preclinical pro-arrhythmia assessment of candidate compounds affecting cardiac ion channels are currently lacking, our approach may comprise a plausible first screening step (27).

Previous studies of drug effects on cardiac tissue relied on pore block models (45), which fail to capture the complex features of drug-channel kinetics that emerge in altered cardiac

rhythms. To reproduce measured drug-channel kinetics, we used a Markovian representation of Na channel gating and a numerical optimization technique to fit model parameters over multiple frequencies and drug concentrations. The model reproduces cellular-level effects of drug-bound channels, namely, a concentration- and pacing-dependent reduction in cellular excitability that is more profound for flecainide than for lidocaine. However, at the cellular level, high therapeutic concentrations of drug and physiological pacing did not reveal any overt pro-arrhythmic potential—cellular excitability was depressed, but excitation was always successful.

In contrast, tissue simulations revealed drug concentrations causing conduction block with both constant pacing and irregular spontaneous stimuli. With constant pacing, conduction block occurred in the therapeutic range for flecainide, but not lidocaine. These results were validated in whole-heart rabbit epicardial optical mapping, which showed both comparable patterns of CV slowing and the frequency- and dose-dependent onset of conduction block.

We also validated the 2D model predictions that ectopic stimuli induce transient reentry in the presence of therapeutically relevant concentrations of flecainide in both rabbit experiments and human virtual ventricle simulations. At relatively low-frequency tachycardia induced by ventricular ectopy (the arrhythmia trigger observed in the CAST study), flecainide proved markedly more potent and arrhythmogenic than lidocaine (3, 4, 14).

The model predictions confirm previous suggestions (11, 33) that anti-arrhythmic cellular-level markers were paradoxically pro-arrhythmic in coupled tissue. Here, we did not investigate faster rates of ventricular tachycardia (>180 BPM) because they cause syncope and hemodynamic compromise on their own, even without drug application (46). Nonetheless, at faster rates, the model would be expected to predict reduced conduction block threshold complicated by additional intrinsic pro-arrhythmic mechanisms.

In patients with HF, our simulations suggest that flecainide combined with reduced I_{Na} (because of the reduced diastolic intervals stemming from APD prolongation) allow for ultraslow Ca^{2+}-supported conduction that promotes development of reentrant arrhythmias even when spontaneous ventricular ectopy occurs outside of the VW (43, 44). Because lidocaine-bound channels recover faster from drug blockade, reentrant rhythms in HF are less persistent than with flecainide. Future studies should systematically investigate specific temporal manifestations of HF (for example, early, mid, and late) and the effects of anatomical pathophysiological changes (for example, scar tissue) in the myocardium and the resultant effects of anti-arrhythmic drug blockade.

Notably, some drugs affect multiple ion channels. Although lidocaine is specific for Na channels (47), flecainide blocks K^+ channels in some species. In rat ventricular myocytes, flecainide blocks I_{to} (48) and I_K with high affinity (48). In guinea pigs, higher concentrations of flecainide blocked I_{Kr}, but not I_{Ks} (49). In other species, flecainide inhibits L-type calcium current (50) and transient outward current (51), but not inward rectifying K^+ current (52, 53). We did not account for specific effects of K^+ channel block by flecainide and lidocaine because effects are species-dependent and human affinities have not been determined. Even so, effects on human K^+ channels would increase APD, slow conduction, and exacerbate conduction block.

Here, we focused on arrhythmia induction by spontaneous ventricular ectopy. We chose this arrhythmia trigger because this situation was observed in the CAST to be associated with worse outcomes when flecainide was present, thus providing a clinical case for simulations and validation (4, 14). However, this is a limitation of the study, because myriad arrhythmogenic situations and triggers exist (46). We also focused exclusively on

ventricular arrhythmias in this study. The mechanisms put forth in this paper must be tested in the context of atrial arrhythmias in which conditions in the atrium would be complicated by the presence of nodal structures and differences in atrial cell electrophysiology (46, 54).

This study represents the first steps toward the construction of an in silico drug screening system that is readily amenable to high-throughput scale-up. The model predictions suggest that relatively simple simulations in two dimensions may be enough to identify potentially pro- or anti-arrhythmic agents. Our approach constitutes a tractable first step in determining which agents merit further testing in higher dimensions and with experiments. Longer term, the framework should be expanded to cover a range of potentially arrhythmogenic situations —in both normal and diseased tissue.

Materials and Methods

Summary

A computational Markov model was formulated via numerical optimization from experimentally derived rate constants that formed the basis for the drug-free Na channel. The model was expanded to account for the interactions between the Na channel and charged and neutral fractions of flecainide and lidocaine. Assumptions for drug access derived from the modulated and guarded receptor hypotheses and included pH-dependent partitioning and clinical effects of Na channel–blocking drugs. The channel model recapitulated many features of Na channel blockade including time- and voltage-dependent recovery, frequency- and use-dependent block, and tonic block. Sensitivity analysis ensured that the model was robust to perturbations. The drug-channel model was incorporated into a computational model of the human ventricular myocyte. The VW for arrhythmia development and arrhythmia probability is from Starmer. Simulations were validated and compared to rabbit epicardial optical mapping experiments and simulations in MRI-based simulated 3D ventricles (33). A complete description of Materials and Methods is presented in the Supplementary Material.

Supplementary Material

Refer to Web version on PubMed Central for supplementary material.

Acknowledgments

Funding: Supported by the American Heart Association (AHA) (grant-in-aid, Western States Affiliate), the Alfred P. Sloan Foundation, and the NIH National Heart, Lung, and Blood Institute (NHLBI) RO1-HL-085592-05 and RO1-HL-085592-S2 (to C.E.C.); NHLBI RO1-HL-56810-16 (to R.S.K.); NHLBI R01-HL-082729 and R01-HL-103428 and National Science Foundation grant CBET-0933029 (to N.A.T.); NIH P30: HL101280-01 (to C.M.R.); Medical Scientist Training Program grant 5 T 32 GM 07739 (to J.D.M.); and AHA 10PRE3650037 (to J.D.B.).

References and Notes

1. Bigger JT Jr, Mandel WJ. Effect of lidocaine on the electrophysiological properties of ventricular muscle and Purkinje fibers. J Clin Invest. 1970; 49:63–77. [PubMed: 5409809]
2. Rosen MR, Hoffman BF. Mechanisms of action of antiarrhythmic drugs. Circ Res. 1973; 32:1–8. [PubMed: 4567446]
3. Preliminary report: Effect of encainide and flecainide on mortality in a randomized trial of arrhythmia suppression after myocardial infarction. The Cardiac Arrhythmia Suppression Trial (CAST) Investigators. N Engl J Med. 1989; 321:406–412. [PubMed: 2473403]
4. Echt DS, Liebson PR, Mitchell LB, Peters RW, Obias-Manno D, Barker AH, Arensberg D, Baker A, Friedman L, Greene HL, Huther ML, Richardson DW, Investigators CAST. Mortality and

morbidity in patients receiving encainide, flecainide, or placebo. The Cardiac Arrhythmia Suppression Trial. N Engl J Med. 1991; 324:781–788. [PubMed: 1900101]

5. Burashnikov A, Antzelevitch C. New developments in atrial antiarrhythmic drug therapy. Nat Rev Cardiol. 2010; 7:139–148. [PubMed: 20179721]
6. Clancy CE, Rudy Y. Linking a genetic defect to its cellular phenotype in a cardiac arrhythmia. Nature. 1999; 400:566–569. [PubMed: 10448858]
7. Noble D. The rise of computational biology. Nat Rev Mol Cell Biol. 2002; 3:459–463. [PubMed: 12042768]
8. Rodriguez B, Burrage K, Gavaghan D, Grau V, Kohl P, Noble D. The systems biology approach to drug development: Application to toxicity assessment of cardiac drugs. Clin Pharmacol Ther. 2010; 88:130–134. [PubMed: 20520607]
9. Hondeghem LM, Katzung BG. Time- and voltage-dependent interactions of antiarrhythmic drugs with cardiac sodium channels. Biochim Biophys Acta. 1977; 472:373–398. [PubMed: 334262]
10. Hille B. Local anesthetics: Hydrophilic and hydrophobic pathways for the drug-receptor reaction. J Gen Physiol. 1977; 69:497–515. [PubMed: 300786]
11. Starmer CF, Lastra AA, Nesterenko VV, Grant AO. Proarrhythmic response to sodium channel blockade. Theoretical model and numerical experiments. Circulation. 1991; 84:1364–1377. [PubMed: 1653123]
12. Hondeghem LM, Katzung BG. Antiarrhythmic agents: The modulated receptor mechanism of action of sodium and calcium channel-blocking drugs. Annu Rev Pharmacol Toxicol. 1984; 24:387–423. [PubMed: 6203481]
13. Balser JR, Nuss HB, Orias DW, Johns DC, Marban E, Tomaselli GF, Lawrence JH. Local anesthetics as effectors of allosteric gating. Lidocaine effects on inactivation-deficient rat skeletal muscle Na channels. J Clin Invest. 1996; 98:2874–2886. [PubMed: 8981936]
14. Greene HL, Roden DM, Katz RJ, Woosley RL, Salerno DM, Henthorn RW. The Cardiac Arrhythmia Suppression Trial: First CAST … then CAST-II. J Am Coll Cardiol. 1992; 19:894–898. [PubMed: 1552108]
15. Colquhoun D, Dowsland KA, Beato M, Plested AJ. How to impose microscopic reversibility in complex reaction mechanisms. Biophys J. 2004; 86:3510–3518. [PubMed: 15189850]
16. Brunton, LL.; Lazo, JS.; Parker, KL. Goodman & Gilman's The Pharmacological Basis of Therapeutics. 11. McGraw-Hill; New York: 2006.
17. Liu H, Atkins J, Kass RS. Common molecular determinants of flecainide and lidocaine block of heart Na^+ channels: Evidence from experiments with neutral and quaternary flecainide analogues. J Gen Physiol. 2003; 121:199–214. [PubMed: 12601084]
18. Zhu Y, Kyle JW, Lee PJ. Flecainide sensitivity of a Na channel long QT mutation shows an open-channel blocking mechanism for use-dependent block. Am J Physiol Heart Circ Physiol. 2006; 291:H29–H37. [PubMed: 16501012]
19. Liu H, Tateyama M, Clancy CE, Abriel H, Kass RS. Channel openings are necessary but not sufficient for use-dependent block of cardiac Na^+ channels by flecainide: Evidence from the analysis of disease-linked mutations. J Gen Physiol. 2002; 120:39–51. [PubMed: 12084774]
20. Abriel H, Wehrens XH, Benhorin J, Kerem B, Kass RS. Molecular pharmacology of the sodium channel mutation D1790G linked to the long-QT syndrome. Circulation. 2000; 102:921–925. [PubMed: 10952963]
21. Nagatomo T, January CT, Makielski JC. Preferential block of late sodium current in the LQT3 ΔKPQ mutant by the class I_C antiarrhythmic flecainide. Mol Pharmacol. 2000; 57:101–107. [PubMed: 10617684]
22. Yue DT, Lawrence JH, Marban E. Two molecular transitions influence cardiac sodium channel gating. Science. 1989; 244:349–352. [PubMed: 2540529]
23. Bennett PB, Valenzuela C, Chen LQ, Kallen RG. On the molecular nature of the lidocaine receptor of cardiac Na^+ channels. Modification of block by alterations in the α-subunit III-IV interdomain. Circ Res. 1995; 77:584–592. [PubMed: 7641328]
24. Wang ZG, Pelletier LC, Talajic M, Nattel S. Effects of flecainide and quinidine on human atrial action potentials. Role of rate-dependence and comparison with guinea pig, rabbit, and dog tissues. Circulation. 1990; 82:274–283. [PubMed: 2114235]

25. Ramos E, O'Leary ME. State-dependent trapping of flecainide in the cardiac sodium channel. J Physiol. 2004; 560:37–49. [PubMed: 15272045]
26. ten Tusscher KH, Panfilov AV. Alternans and spiral breakup in a human ventricular tissue model. Am J Physiol Heart Circ Physiol. 2006; 291:H1088–H1100. [PubMed: 16565318]
27. Lu HR, Rohrbacher J, Vlaminckx E, Van Ammel K, Yan GX, Gallacher DJ. Predicting drug-induced slowing of conduction and pro-arrhythmia: Identifying the 'bad' sodium current blockers. Br J Pharmacol. 2010; 160:60–76. [PubMed: 20331615]
28. Yabek SM, Kato R, Ikeda N, Singh BN. Effects of flecainide on the cellular electrophysiology of neonatal and adult cardiac fibers. Am Heart J. 1987; 113:70–76. [PubMed: 3099562]
29. Borchard U, Boisten M. Effect of flecainide on action potentials and alternating current-induced arrhythmias in mammalian myocardium. J Cardiovasc Pharmacol. 1982; 4:205–212. [PubMed: 6175802]
30. Shaw RM, Rudy Y. Ionic mechanisms of propagation in cardiac tissue. Roles of the sodium and L-type calcium currents during reduced excitability and decreased gap junction coupling. Circ Res. 1997; 81:727–741. [PubMed: 9351447]
31. Starmer CF, Lastra AA, Nesterenko VV, Grant AO. Proarrhythmic response to sodium channel blockade. Theoretical model and numerical experiments. Circulation. 1991; 84:1364–1377. [PubMed: 1653123]
32. Ermis C, Zhu AX, Vanheel L, Lemke MJ, Sakaguchi S, Lurie KG, Lu F, Lin J, Benditt DG. Comparison of ventricular arrhythmia frequency in patients with ischemic cardiomyopathy versus nonischemic cardiomyopathy treated with implantable cardioverter defibrillators. Am J Cardiol. 2005; 96:233–238. [PubMed: 16018849]
33. Starmer CF. How antiarrhythmic drugs increase the rate of sudden cardiac death. Int J Bifurcat Chaos. 2002; 12:1953–1968.
34. Mines GR. On circulating excitations in heart muscles and their possible relation to tachycardia and fibrillation. Trans R Soc Can. 1914; 4:43–52.
35. Allessie MA, Bonke FI, Schopman FJ. Circus movement in rabbit atrial muscle as a mechanism of trachycardia. Circ Res. 1973; 33:54–62. [PubMed: 4765700]
36. Starmer CF, Biktashev VN, Romashko DN, Stepanov MR, Makarova ON, Krinsky VI. Vulnerability in an excitable medium: Analytical and numerical studies of initiating unidirectional propagation. Biophys J. 1993; 65:1775–1787. [PubMed: 8298011]
37. Bray MA, Wikswo JP. Considerations in phase plane analysis for nonstationary reentrant cardiac behavior. Phys Rev E Stat Nonlin Soft Matter Phys. 2002; 65:051902. [PubMed: 12059588]
38. Panfilov AV. Is heart size a factor in ventricular fibrillation? Or how close are rabbit and human hearts? Heart Rhythm. 2006; 3:862–864. [PubMed: 16818223]
39. Priebe L, Beuckelmann DJ. Simulation study of cellular electric properties in heart failure. Circ Res. 1998; 82:1206–1223. [PubMed: 9633920]
40. Beuckelmann DJ, Näbauer M, Erdmann E. Alterations of K^+ currents in isolated human ventricular myocytes from patients with terminal heart failure. Circ Res. 1993; 73:379–385. [PubMed: 8330380]
41. Glukhov AV, Fedorov VV, Lou Q, Ravikumar VK, Kalish PW, Schuessler RB, Moazami N, Efimov IR. Transmural dispersion of repolarization in failing and nonfailing human ventricle. Circ Res. 2010; 106:981–991. [PubMed: 20093630]
42. Lou Q, Fedorov VV, Glukhov AV, Moazami N, Fast VG, Efimov IR. Transmural heterogeneity and remodeling of ventricular excitation-contraction coupling in human heart failure. Circulation. 2011; 123:1881–1890. [PubMed: 21502574]
43. Rohr S, Kucera JP, Kléber AG. Slow conduction in cardiac tissue, I: Effects of a reduction of excitability versus a reduction of electrical coupling on microconduction. Circ Res. 1998; 83:781–794. [PubMed: 9776725]
44. Wang Y, Rudy Y. Action potential propagation in inhomogeneous cardiac tissue: Safety factor considerations and ionic mechanism. Am J Physiol Heart Circ Physiol. 2000; 278:H1019–H1029. [PubMed: 10749693]
45. Brennan T, Fink M, Rodriguez B. Multiscale modelling of drug-induced effects on cardiac electrophysiological activity. Eur J Pharm Sci. 2009; 36:62–77. [PubMed: 19061955]

46. Marchlinski, F. The tachyarrhythmias, in Harrison's Principles of Internal Medicine. 17. Fauci, AS.; Braunwald, E.; Kasper, DL.; Hauser, SL.; Longo, DL.; Jameson, JL.; Loscalzo, J., editors. McGraw-Hill; New York: 2008.
47. Burton, LL.; Chabner, BA.; Knollan, BC. Goodman & Gilman's The Pharmacological Basis of Therapeutics. 12. McGraw-Hill; New York: 2010.
48. Slawsky MT, Castle NA. K+ channel blocking actions of flecainide compared with those of propafenone and quinidine in adult rat ventricular myocytes. J Pharmacol Exp Ther. 1994; 269:66–74. [PubMed: 8169853]
49. Wang DW, Kiyosue T, Sato T, Arita M. Comparison of the effects of class I anti-arrhythmic drugs, cibenzoline, mexiletine and flecainide, on the delayed rectifier K^+ current of guinea-pig ventricular myocytes. J Mol Cell Cardiol. 1996; 28:893–903. [PubMed: 8762029]
50. Scamps F, Undrovinas A, Vassort G. Inhibition of ICa in single frog cardiac cells by quinidine, flecainide, ethmozin, and ethacizin. Am J Physiol. 1989; 256:C549–C559. [PubMed: 2538064]
51. Wang Z, Fermini B, Nattel S. Mechanism of flecainide's rate-dependent actions on action potential duration in canine atrial tissue. J Pharmacol Exp Ther. 1993; 267:575–581. [PubMed: 8246130]
52. Yamashita T, Nakajima T, Hamada E, Hazama H, Omata M, Kurachi Y. Flecainide inhibits the transient outward current in atrial myocytes isolated from the rabbit heart. J Pharmacol Exp Ther. 1995; 274:315–321. [PubMed: 7616415]
53. Follmer CH, Cullinan CA, Colatsky TJ. Differential block of cardiac delayed rectifier current by class Ic antiarrhythmic drugs: Evidence for open channel block and unblock. Cardiovasc Res. 1992; 26:1121–1130. [PubMed: 1291091]
54. Hatem SN, Coulombe A, Balse E. Specificities of atrial electrophysiology: Clues to a better understanding of cardiac function and the mechanisms of arrhythmias. J Mol Cell Cardiol. 2010; 48:90–95. [PubMed: 19744488]

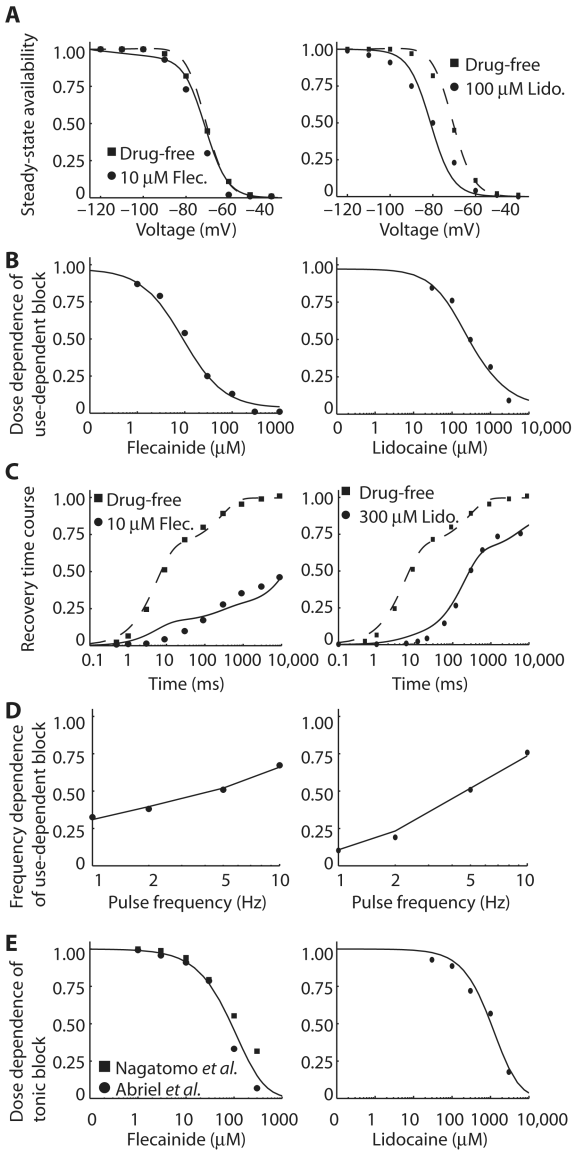

Fig. 1.

Simulated and experimental drug–Na channel interactions. Black and dotted lines depict the results of simulation; the symbols represent experimental data. (**A**) Steady-state channel availability. Currents measured at −10 mV with 10 μM flecainide (Flec.) (left) or 100 μM lidocaine (Lido.) (right) pulsed from −120 to −40 mV in 5-mV increments (normalized to tonic block at −120 mV) (17). (**B**) Dose dependence of use-dependent block (UDB) from 300 pulses to −10 mV for 25 ms from −100 mV at 5 Hz with indicated drug dose (20). Peak current at last pulse normalized to first [note that in drug-free condition, 2.8% loss of current occurs during the pulse protocol (because of inactivation and rundown), so the normalized value is 0.97]. (**C**) Recovery from UDB after pulses (to −10 mV for 25 ms at 25 Hz) from −100 mV with 10 μM flecainide (19) (left) or 300 μM lidocaine (right). Test pulses (−10 mV) were after variable recovery intervals at −100 mV. Currents were normalized to tonic block. (**D**) Frequency dependence of UDB. Protocol is the same as in (B) with 10 μM flecainide (19) (left) or 300 μM lidocaine (20) (right). (**E**) Dose dependence of tonic block evoked by depolarizing pulse from −100 to −10 mV. Block is peak current normalized to drug-free conditions.

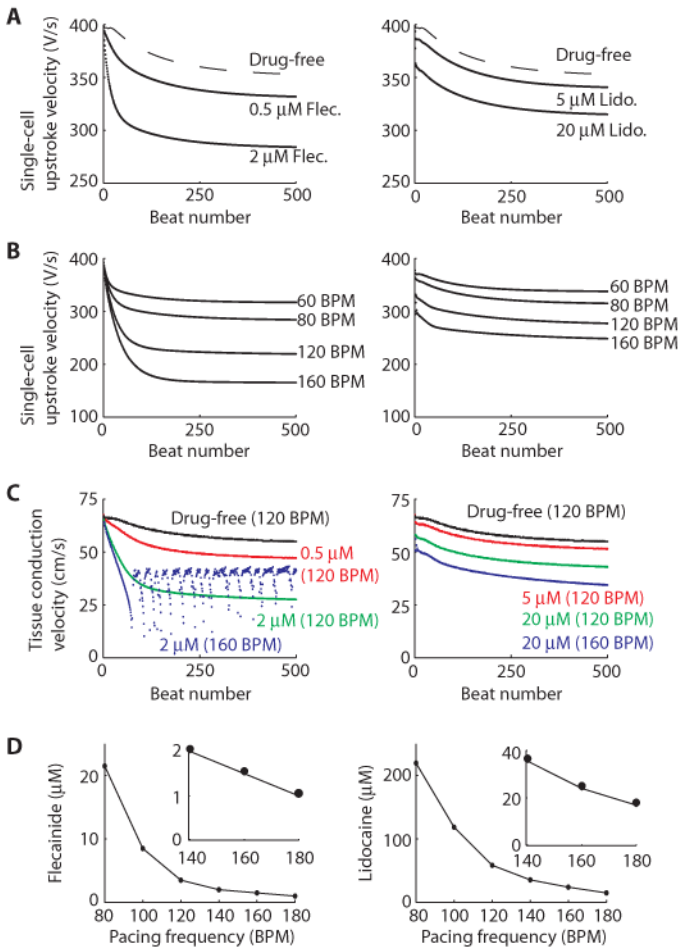

Fig. 2.

Effects of flecainide and lidocaine on cell excitability and conduction velocity in a human ventricular cell model (26). (**A**) Effects of 0.5 or 2 μM flecainide (Flec.) (left) and 5 or 20 μM lidocaine (Lido.) (right) as indicated on single-cell upstroke velocity (V/s) paced at 80 BPM. (**B**) Effects of 2 μM flecainide (left) and 20 μM lidocaine (right) on upstroke velocity (V/s) at the indicated frequency. (**C**) Effects of 0.5 μM (120 BPM) and 2 μM (120 and 160 BPM) flecainide (left) and 5 μM (120 BPM) and 20 μM (120 and 160 BPM) lidocaine (right) on conduction velocity in 1D tissue. (**D**) Minimum concentrations of flecainide (left) and lidocaine (right) required for conduction block at the indicated pacing frequencies.

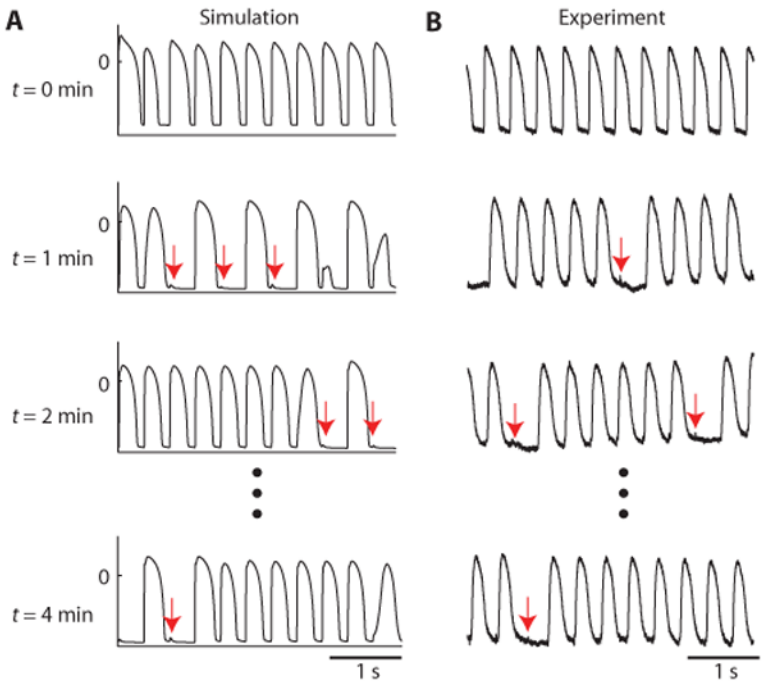

Fig. 3.

Complex dynamics in simulations and experiments with 2 μM flecainide at 160 BPM. (**A**) The extended time course of simulated action potentials (2 μM flecainide at 160 BPM) at 1, 2, and 4 min after addition of drug. Action potentials from cell 50 are shown. (**B**) Experimental action potentials in the rabbit epicardium paced at 160 BPM with 2 μM flecainide. Red arrows indicate failed stimuli.

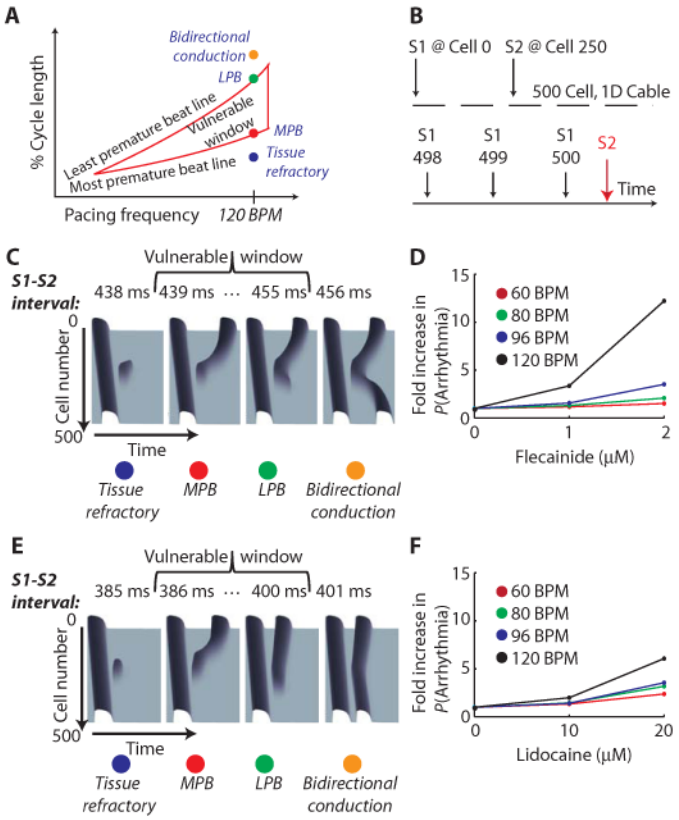

Fig. 4.

Prediction of arrhythmia propensity by the vulnerable window (VW). (**A**) Schematic for the VW protocol. (**B**) Schematic for the pacing protocol. (**C**) VW with 2 μM flecainide after pacing (S1) at 120 BPM. Cell position is shown on the y axis. The x axis indicates time and the z axis indicates voltage, with darker color indicating more depolarized potentials and light gray indicating repolarized tissue. An additional stimulus (S2) applied at cell 250 before the VW (blue dot) fails to excite refractory tissue (left). Premature impulses applied at the most premature beat (MPB) (red dot) and least premature beat (LPB) (green dot) cause arrhythmogenic unidirectional retrograde conduction. An impulse applied after the VW (orange dot) causes bidirectional conduction. (**D**) The Starmer metric, *P*(Arrhythmia) (33), was used to calculate arrhythmia susceptibility to 0 to 2 μM flecainide normalized to drug-free risk. (**E**) VW for lidocaine (20 μM) after pacing at 120 BPM. Abbreviations as for (C). (**F**) The Starmer metric, *P*(Arrhythmia) (33), was used to calculate arrhythmia susceptibility to 0 to 20 μM lidocaine normalized to drug-free risk.

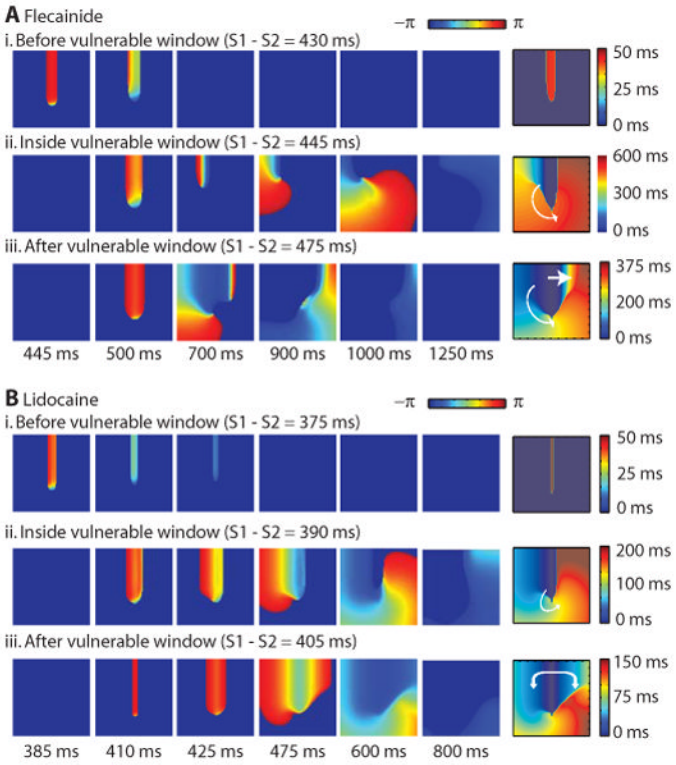

Fig. 5.

Effects of flecainide and lidocaine in a 2D cardiac tissue model. (A and B) Phase maps for (**A**) flecainide (2 μM) and (**B**) lidocaine (20 μM) at times as indicated under panels [scale above: red indicates wavefront and blue indicates fully repolarized (but not necessarily recovered from drug block) tissue]. Panels at right are the corresponding activation isochrones (time scale on right). A premature impulse was applied in the wake of the preceding wave (i) before the vulnerable window (VW), (ii) within the VW, or (iii) after the VW for flecainide (**A**) or lidocaine (**B**). See the Supplementary Material for the schematic of pacing protocol.

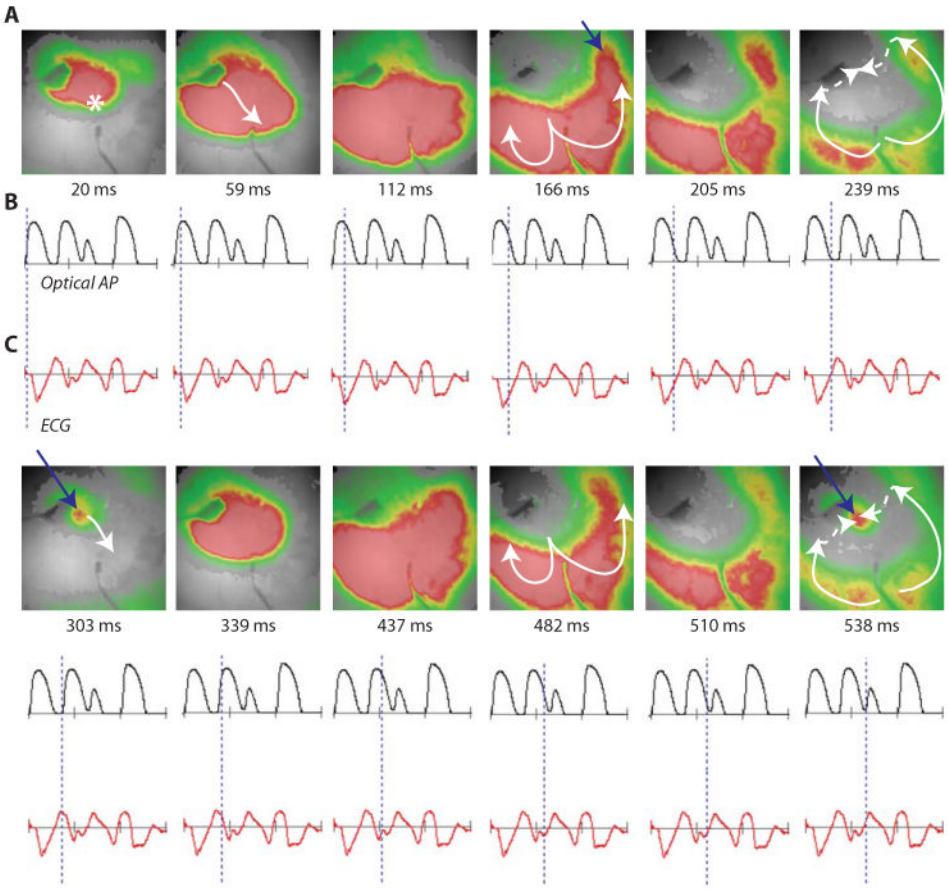

Fig. 6.

Experimental validation of reentrant behavior with flecainide. (**A**) Snapshots of a nonsustained salvo transmural figure-of-eight reentry induced after rapid pacing with 2 μM flecainide. Electrode pacing site is denoted with an asterisk. (**B**) Optical action potential (AP). (**C**) Electrocardiogram (ECG) recording. Dashed blue line indicates time in (**A**). After pacing, a reentrant figure-of-eight wave breaks through in the top left field of view and travels down and to the right before spiraling back around. The blue arrows show the tip of the wave first traveling endocardially and then reentering into recovered epicardium (top left of tissue). The white solid arrows show the epicardial trajectory of the wave, whereas the dotted white arrows show the projected transmural path.

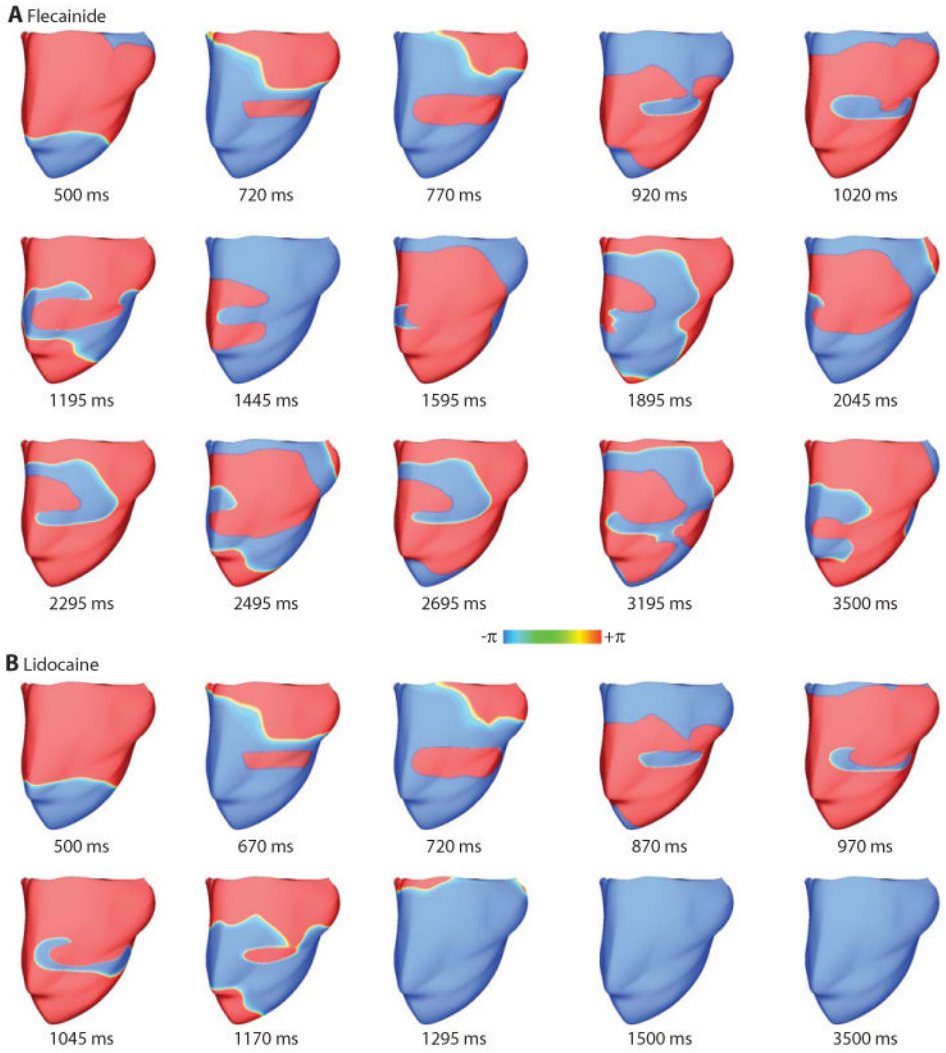

Fig. 7.

Reentry in 3D models of the human ventricle. (**A**) Phase map of a sustained figure-of-eight reentry with 2 μM flecainide paced at 120 BPM. (**B**) Phase map of nonsustained reentry with 20 μM lidocaine paced at 120 BPM. The S1-S2 interval was 720 ms for flecainide and 670 ms for lidocaine. Sustained reentry occurred when applying S2 within the vulnerable window of the model with 2 μM flecainide (VW = 660 to 735 ms), but not for 20 μM lidocaine (VW = 630 to 685 ms).

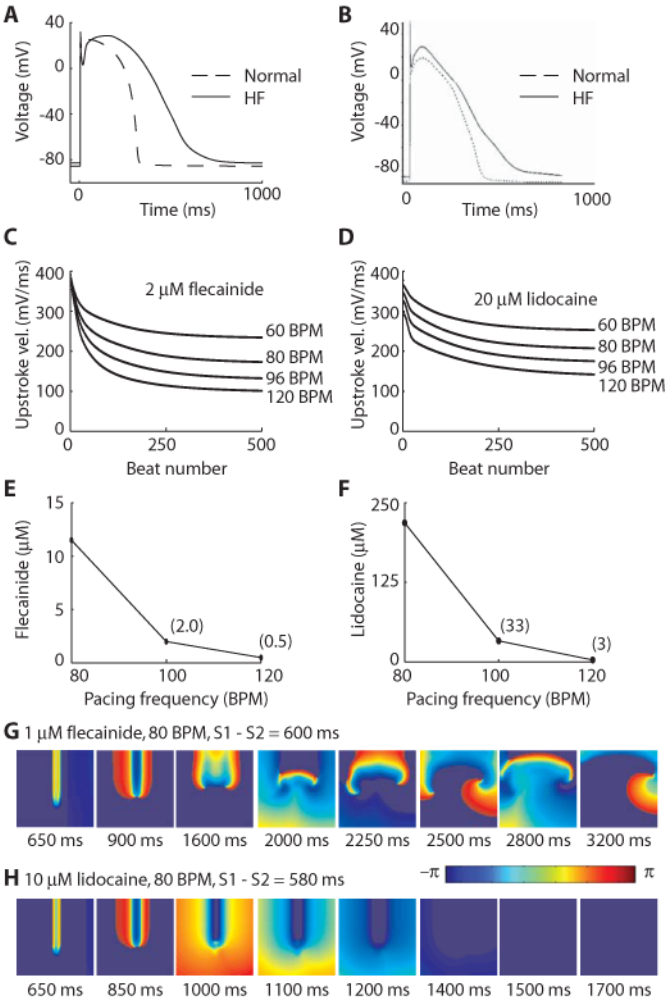

Fig. 8.

Drug effects in heart failure (HF). (**A**) The HF APD is prolonged and exhibits diastolic depolarization. (**B**) Results from Priebe and Beuckelmann, comparable to those in (A) (39). (**C**) For flecainide, the single uncoupled cellular upstroke velocity is shown for indicated frequencies. (**D**) For lidocaine, the single uncoupled cellular upstroke velocity is shown for indicated frequencies. (**E**) For flecainide, the minimum drug concentrations (in parentheses) required for conduction block are shown at indicated frequencies. (**F**) For lidocaine, the minimum drug concentrations (in parentheses) required for conduction block are shown at indicated frequencies. (**G** and **H**) Reentrant dynamics for half-maximal drug concentration (1 μM flecainide, 10 μM lidocaine) at 80 BPM. Shown are phase maps at indicated times.